Experimental studies of wall interactions of adsorbed spin-polarized ^{131}Xe nuclei

Z. Wu,* W. Happer, M. Kitano,† and J. Daniels‡
Department of Physics, Princeton University, Princeton, New Jersey 08544
(Received 26 April 1990)

We have made a quantitative study of nuclear spin relaxation of ^{131}Xe atoms adsorbed on the surface of glass cells. By using highly asymmetric glass cells we have increased the wall-induced quadrupole splitting of the nuclear-spin sublevels of ^{131}Xe atoms by almost two orders of magnitude over previously reported values. These large surface interactions were used to extract quantitative information about the electric-field gradients experienced by the nuclei of ^{131}Xe atoms adsorbed on the glass surface and about the activation energies for surface adsorption. The experimental results indicate that the electric-field gradients at any surface site are nearly isotropic. The residual nonzero mean value of the fluctuating field gradient has cylindrical symmetry about the normal direction to the surface. The mean-field gradient along the surface normal direction is only 2.3% as large as the rms value. We find that silicone wall coatings, which slow down the relaxation of ^{129}Xe nuclear spins, speed up the relaxation of ^{131}Xe nuclear spins. This may be due to the nuclear quadrupole interactions of ^{131}Xe atoms dissolved in the relatively thick silicone wall coatings. Measurements of the temperature dependence of the coherent wall interaction show that the activation energy ($\approx$0.03 eV) for the coherent wall interaction in well-cured, hydrogen-free cells is about three times smaller than the activation energy ($\approx$0.10 eV) in hydrided cells.

I. INTRODUCTION

The interactions between nuclear-spin polarized diamagnetic atoms and surfaces cause a number of interesting phenomena. For example, Simpson and co-workers[1,2] observed that the relaxation rate of the spin-3/2 nuclei of ^{201}Hg depends on the asymmetry of the quartz cell used to contain the Hg vapor and on the orientation of the cell with respect to the external magnetic field. Simpson[2] also observed the beating signal in ^{201}Hg, which is caused by the shift in the nuclear magnetic-resonance frequencies of ^{201}Hg. Similar effects were observed by Volk and co-workers[3,4] for spin-polarized ^{83}Kr and ^{131}Xe nuclei. However, no such phenomena have been observed for ^{199}Hg and ^{129}Xe, which do not have nuclear quadrupole moments. The most obvious explanation for these phenomena is that they are caused by the quadrupole interactions between the nuclear spins of the adsorbed atoms and the electric-field gradients at the wall. The nuclear-spin relaxation rate has comparable contributions from gas-phase and surface interactions, and these are difficult to separate in the experimental data. In contrast, the beating signals due to the coherent quadrupole interaction are unaffected by gas-phase interactions and are therefore an ideal probe of purely surface interactions.

In this paper we will report the results of quantitative experimental studies of the wall interactions of spin-polarized ^{131}Xe nuclei. The relaxation of ^{131}Xe can be conveniently compared, in the same cell, to that of ^{129}Xe, which has a spin-1/2 nucleus and relaxes because of magnetic dipole interactions. By using highly asymmetric cells, we increased the wall-induced frequency shift by two orders of magnitude over the previously reported values. These large frequency shifts let us study in a systematic way various properties of the electric-field gradients at the glass surface which are responsible for the NMR frequency shift and the relaxation of the spin-polarized ^{131}Xe nuclei. We also report the first study of the effect of wall coating on spin-polarized ^{131}Xe nuclei. The results indicate that silicon-coated glass surfaces are strongly depolarizing for ^{131}Xe nuclei, in sharp contrast to the case of ^{129}Xe, for which nuclear-spin relaxation is slower in cells with silicone wall coatings.

The theory of nuclear spin relaxation of diamagnetic atomic gases due to incoherent quadrupolar wall interactions was first developed by Cohen-Tannoudji[5] in connection with his studies of the spin relaxation of ^{201}Hg. Following a suggestion by Happer, a semiquantitative theory of coherent wall interactions of noble gas nuclei was developed by Volk and co-workers.[3,4] Generalizing work by Massnou-Seeuws and Bouchiat,[6] Wu *et al.*[7] developed a more complete, perturbative theory of wall interactions, with special emphasis on coherent quadrupolar interactions. Since we will discuss our experiments within the framework of that theory, we will briefly review the key theoretical ideas here.

The nuclear-spin Hamiltonian of a noble-gas atom in a gas cell can be written as

$$H = H_b + H_w \ . \tag{1}$$

Here

$$H_b = g_K \mu_B B_0 K_z = \hbar \omega_0 K_z \tag{2}$$

is the gas-phase or bulk interaction Hamiltonian and $\omega_0 = g_K \mu_B B_0 / \hbar$ is the Larmor frequency in the homogeneous, static field B_0, which is in the z direction. The nuclear spin of the noble gas atom is $\mathbf{K}$. The wall interaction Hamiltonian H_w (considering only the quadrupolar part) can be written as

$$H_w = \frac{1}{6}\sum_{i,j} Q_{ij}\frac{\partial^2 V_w}{\partial x_i \partial x_j} = \frac{2\hbar}{3(2K-1)}\mathbf{K}\cdot\dot{\overleftrightarrow{\Theta}}\cdot\mathbf{K} \ . \tag{3}$$

The electric-field gradients $\partial V_w/\partial x_i \partial x_j$, which depolarize the nuclei of adsorbed atoms through interactions with the quadrupole moment tensor Q_{ij}, are produced by polar groups near the surface, e.g., —OH or —ONa, by the conduction-band electrons at the metal surfaces, etc. The zeroth-order field gradient calculated for the ^{131}Xe nucleus at the wall may be modified substantially as a result of Sternheimer shielding or antishielding by core electrons.[8] These microscopic field gradients will fluctuate in time due to the relative motions of the adsorbed atoms and the atoms of the surface, and due to the fluctuations in the degenerate electron gas of metal surfaces on which the atoms may be adsorbed. Important quadrupolar interactions may also occur for atoms dissolved in the relative thick films of wall coatings. As indicated in (3), it is convenient to write the quadrupole interaction in terms of a traceless, symmetric, twist-rate tensor $\dot{\overleftrightarrow{\Theta}}$, defined by Eq. (96) of Ref. 7, and which we will discuss in more detail later.

The microscopic effects of the quadrupole wall interactions are characterized by two parameters $\langle\theta\rangle$ and $\langle\theta^2\rangle$. Suppose that a ^{131}Xe atom is adsorbed on a part of the wall where the macroscopic surface is normal to the unit vector $\mathbf{n}$. While the atom is stuck to the wall, the nuclear-spin polarization will be twisted, on the average, through the angle

$$\langle\theta\rangle = \left\langle \int_0^\tau \mathbf{n}\cdot\dot{\overleftrightarrow{\Theta}}\cdot\mathbf{n}\, dt \right\rangle , \tag{4}$$

as discussed in connection with Eq. (99) of Ref. 7. While the atom is adsorbed, it will move from site to site across the surface and the field gradients will fluctuate in sign, so the mean twist angle (4) may be the small residual of much larger positive and negative twist angles. A measure of the instantaneous quadrupole interaction is the mean-squared twist angle

$$\langle\theta^2\rangle = 5\frac{\tau_c\tau_s^2}{\tau_c+\tau_s}\left\langle (\mathbf{z}\cdot\dot{\overleftrightarrow{\Theta}}\cdot\mathbf{z})^2 \right\rangle , \tag{5}$$

which was discussed in connection with Eq. (111) of Ref. 7. Here $\tau_s = \langle\tau\rangle$ is the mean dwell time of a Xe atom on the surface, τ_c is the correlation time of the fluctuating field gradient, and $\mathbf{z}$ is a unit vector along the z axis of the laboratory-fixed coordinate system. The factor of 5 comes from the assumption in Ref. 7 that the field gradients are nearly isotropic and the Larmor period of the nuclei is long compared to τ_c. Then each of the five independent components of the twist-rate tensor contributes an equal amount to the relaxation. Our data, which we will discuss in detail below, show that $\langle\theta^2\rangle \gg \langle\theta\rangle^2$, so the assumption of near isotropy is confirmed by observation. The assumption of near isotropy is equivalent to the assumption that the twist-rate tensor is almost a multiple of the unit matrix. Therefore the unit vector $\mathbf{z}$ in (5) can almost be replaced by any real unit vector.

The theory of Ref. 7 is based on a perturbation expansion in powers of the wall interaction. The expansion parameter is on the order of $l\lambda^{-1}\langle\theta\rangle$, where λ is the mean free path of spin-polarized gas atoms, l is a characteristic linear dimension of the cell. For the conditions of our experiments where the gas pressures were a few tens of Torr, $\lambda \approx 10^{-3}$ cm, the cell dimension were $l \approx 0.5$ cm, the mean twist angle, defined by (4), turns out to be $\langle\theta\rangle \approx 4\times10^{-5}$. Thus the expansion parameter is on the order of 0.02, and the perturbative theory of Ref. 7 should work very well. A preliminary description of some parts of this work has already been published.[9]

II. EXPERIMENT

The experimental arrangement for studying the wall interactions of ^{131}Xe is shown in Fig. 1. Our experimental method is simpler than the ones used in previous experiments.[3,4] It requires only moderate magnetic shielding. The signal is detected by using the circular dichroism induced in the attenuation coefficient of Rb resonance light by the spin-polarized noble-gas nuclei.[10] An important new procedure, which we used in this experiment, was to actively lock the longitudinal magnetic field to a long-term stability of about 2 μG. This stability in the longitudinal magnetic field allowed us to study the small shift in the nuclear magnetic-resonance frequency of ^{131}Xe due to the wall interactions.

A. Sample cell preparation

The sample cells were made of Pyrex glass and were cylindrical in shape, with diameter d and height h. The diameters d were about 1.3 cm and the height h varied between 0.3 and 1 cm. The procedures for filling the cells were similar to those described by Zeng *et al.*[10] The cells contained a few milligrams of Rb metal, 5 Torr of ^{131}Xe (isotopically enriched to an assay of 70 at. % of ^{131}Xe and 10 at. % of ^{129}Xe), and various pressures of N_2. All the partial pressures are quoted at a temperature of 25 °C.

B. Magnetic field stabilization

As indicated in Fig. 1(a), a static magnetic field B_0 of about 0.1 G in the direction of the z axis was produced by a solenoid 97 cm long and 30 cm in diameter. The solenoid was located inside a soft-iron flux return cylinder. These were surrounded with two concentric μ-metal magnetic shields, which reduced the field fluctuation to less than 1 mG. Care was taken to avoid having any magnetic materials near the cell. In Fig. 1(b) is shown an optically pumped Cs magnetometer,[11] which in conjunction with a feedback system actively stabilized the longitudinal magnetic field to within 2 μG. The magnetometer was located within 3 cm of the cell. We chose a cesium magnetometer because it is advantageous to have the magnetometer operate at a frequency different from the Rb resonance frequency, and the high vapor pressure of Cs makes it possible for the magnetometer to operate at a relatively low temperature, which will not damage fiber bundles, plastic circular polarizer, etc., used in the apparatus.

As shown in Fig. 1(b), the 1-MHz square wave output from a frequency synthesizer (HP 3133 A) is converted into a sinusoidal wave of frequency $\nu_0 = \frac{1}{26}$ MHz modu-

lated at $\nu_m = 137$ Hz, with the aid of a frequency divider, a modulator, and a filter. This sinusoidal wave is then fed into the rf coils of the Cs magnetometer. The rf coils are positioned so that they produce an oscillating magnetic field in the y direction. The D_1 light from a Cs resonance lamp, guided by a fiber bundle, passes through a circular polarizer and illuminates the Cs cell, which is a spherical Pyrex-glass bubble with a diameter of 0.9 cm, containing a few milligrams of Cs metal and 50 Torr of N_2 gas. The transmitted Cs light is detected by a silicon photodiode, a preamplifier, and a lock-in amplifier, which is tuned to the frequency ν_m.

Due to the modulation of the rf, the intensity of the transmitted light was modulated at the frequency ν_m with an amplitude proportional to

$$\frac{a\Delta^2}{2}\frac{\nu-\nu_0}{[(\nu-\nu_0)^2+(\Delta/2)^2]^2}, \tag{6}$$

where a is the modulation amplitude and Δ is the full width at half-maximum (FWHM) of the magnetic resonance line, which in our case was ~ 1 kHz. At the ~ 0.1

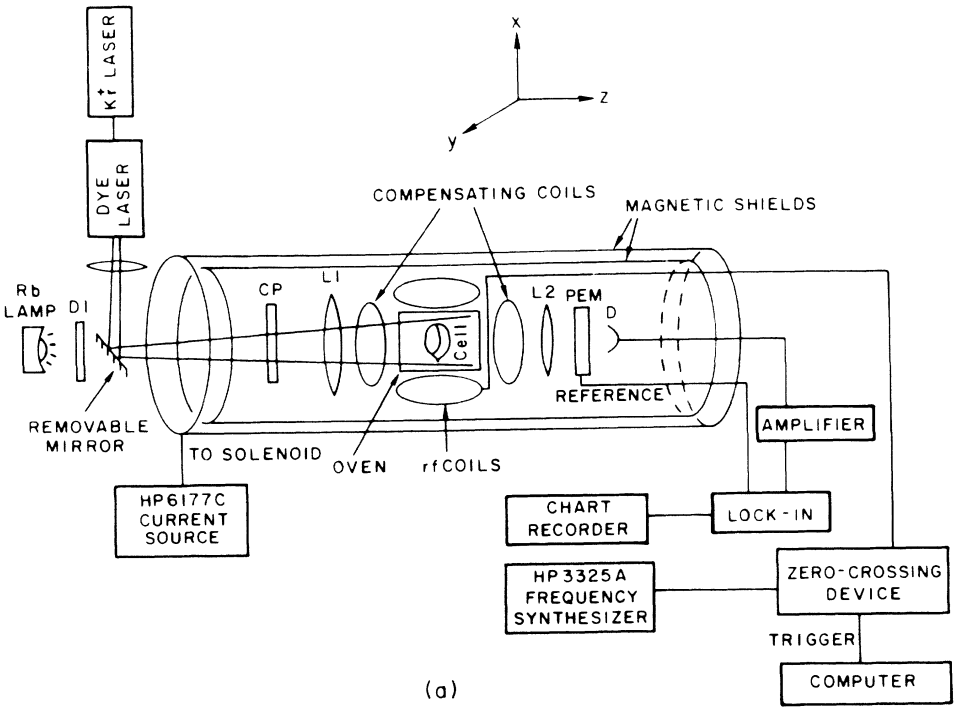

FIG. 1. (a) Experimental arrangement to study the wall interactions of spin-polarized ^{131}Xe nuclei. The nuclear polarization of ^{131}Xe is produce by spin exchange with optically pumped Rb atoms. (b) Schematic diagram for the Cs magnetometer used to stabilize the longitudinal magnetic field.

G field which we used, the Zeeman lines of Cs are not resolved, the separation between adjacent lines being ~0.27 Hz. At higher fields one could lock the field to an individual Zeeman line. The error signal (6) from the lock-in amplifier drove the proportional-integral feedback circuit shown in Fig. 2, which generated a compensating current to cancel any field fluctuations and lock the field to a value B_0 (~0.1 G), which corresponds to the Larmor frequency $\omega_0=2\pi\nu_0$ of the Cs atoms.

C. Experimental procedures

The wall interactions of ^{131}Xe are observed with the help of transient nuclear-magnetic resonance. The sample cell is placed in an oven and heated to temperatures in the range of 80–100 °C by flowing hot air. A laser beam (7948 Å and ~400 mW) from a cw dye laser, pumped by a krypton-ion laser, after being expanded by a lens, is reflected by a removable mirror through a circular polarizer (CP) and into the cell. The Fresnel lens (L1) had a small hole in the middle so that the laser beam could pass through L1 without being distorted. The Xe nuclei are polarized by spin exchange with Rb atoms, which are maintained nearly fully spin polarized by the circularly polarized laser beam. The Xe nuclear polarization attains its saturation value after a few minutes of pumping. Once the nuclei have been polarized, the laser beam is blocked, the CP removed, and so is the removable mirror. The spin polarization is probed by passing unpolarized 7948-Å D_1 light from a Rb resonance lamp through the cell. This light then passes through a photoelastic modulator, made by Hinds International, and a linear polarizer oriented at 45° to the compression axis of the modulator, before being detected by a silicon photodiode. As discussed by Wu *et al.*,[12] this arrangement is an oscillating circular analyzer which allows one to monitor the small circular polarization of the probe light, due to the longitudinal Rb electronic polarization, which in turn is proportional to the longitudinal polarization $\langle K_z \rangle$ of ^{131}Xe atoms.

At the beginning of the probe phase, we apply a magnetic field of the form $2B_1\cos(\omega t)$ along the x axis. A typical value of B_1 used in this experiment is ~1.37 mG, although larger values of B_1 were used for cells with larger quadrupole splitting. The current that produces this oscillating magnetic field is provided by a frequency synthesizer in conjunction with a zero-crossing trigger,

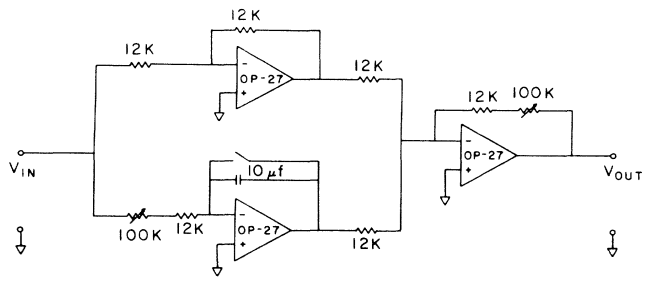

FIG. 2. Proportional-integral (PI) feedback circuit used to actively stabilize the longitudinal magnetic field.

which ensures that the oscillating field always starts at zero amplitude, thus minimizing any possible transient eddy current which might have some depolarizing effect on the Xe polarization. The zero-crossing trigger makes little difference in our results. The oscillating field can be thought of as the vector sum of two fields of magnitude B_1, rotating uniformly at the angular velocities ω and $-\omega$ around z axis.

For a coordinate system rotating at the frequency ω about the static field B_0, the nuclei will precess at the frequency

$$\Omega_0=[(\omega_0-\omega)^2+\omega_1^2]^{1/2}\,, \tag{7}$$

where ω_1, the Rabi frequency, is the Larmor frequency about the field B_1, and ω_0 is the Larmor frequency about the static field B_0. The precession axis $\hat{\xi}$ is tilted by an angle

$$\psi=\cos^{-1}\left[\frac{\omega_0-\omega}{\Omega_0}\right] \tag{8}$$

from the static magnetic field B_0, which defines the z axis. The cell appears to rotate backwards about the z axis at a frequency ω, but since the rotational symmetry axis of the cell coincides with z axis, the cell is effectively at rest in the rotating coordinate system and any slight structural asymmetries, for example, the asymmetry due to the sealing off of the cell, are averaged out. A more detailed description of magnetic-resonance phenomena in the rotating coordinate system can be found in the book by Slichter.[13]

A typical transient signal is shown in Fig. 3(a). This signal was taken in a cylindrical Pyrex-glass cell, 1.28 cm in diameter and 0.68 cm in height, which contained natural Rb metal, 5 Torr of xenon, isotopically enriched to an assay of 70 at. % ^{131}Xe and 10 at. % ^{129}Xe and 50 Torr N_2 gas. The oscillating magnetic field was turned on at time $t=0$, and the oscillation frequency ω was chosen to be equal to the magnetic-resonance frequency ω_0 so that the tilt angle was $\psi=90°$. The fast oscillation is the Larmor precession in the rotating coordinate system at the radian frequency $\Omega_0=\omega_1$. The Fourier transform of the transient signal of Fig. 3(a) is shown in Fig. 3(b). Note that the transient is composed of a "carrier" frequency at 476.3 mHz and "sidebands" with frequencies 443.2 and 506.5 mHz. As indicated in Fig. 3(b), these frequencies can be identified with transitions between Zeeman sublevels of the ^{131}Xe nucleus in the rotating coordinate system. The sidebands are shifted by nearly equal frequency increments above and below the carrier. We define the radian-frequency separation of the upper and lower sidebands for experiments like that of Fig. 3 to be the *quadrupole splitting* frequency $\Delta\Omega_0$.

III. RESULTS

A. Curing of the glass surface

We find that Pyrex-glass surface reach a equilibrium or "cured" state after exposure to Rb-metal vapor for several days at a temperature of about 80 °C. Once the

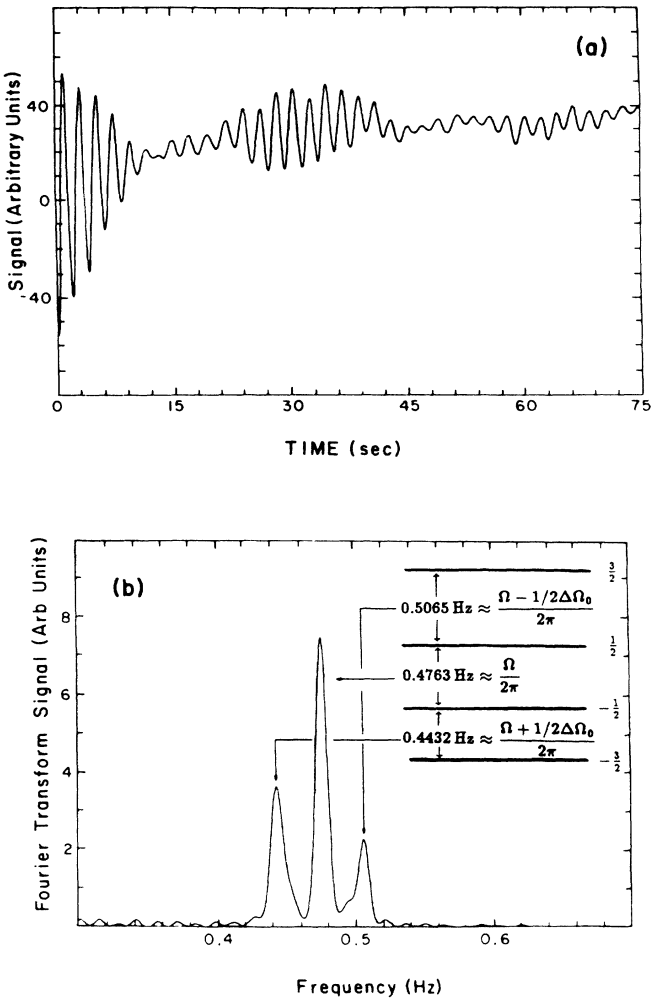

FIG. 3. (a) Precession signal (raw data) of ^{131}Xe for the cell described in the text. The signal is proportional to $\langle K_z \rangle$, the longitudinal nuclear spin of ^{131}Xe in the laboratory coordinate system. (b) The Fourier spectrum of the signal in (a), and the energies of the nuclear-spin sublevels in the rotating coordinate system. The three resonances are peaked at the Bohr frequencies of the three $\Delta m = 1$ transitions.

surface is cured, the beat period and relaxation rate reach a value which is independent of the initial distribution of Rb metal on the surface. The beat period then depends only on the cell geometry and temperture. The curing process is illustrated in Fig. 4, where the evolution of the beat period with time is shown. The circles are the beat period measured in a cell as it is being cured at 82 °C. At the beginning of the curing, the beat period was too long to be observed. After about 150 h of curing, the period reached a constant value (35 sec), which did not change with further curing. We took the cell out of the oven and redistributed the Rb-metal droplets on the wall using a torch and then put it back into the oven and remeasured the beat period, which is labeled by triangles. After torching, the beat period again evolved with time, but to a much lesser extent than for the newly manufactured cell. The beat period approached the same 35-sec period as before, but less time (~90 h) was required for equilibration. The relaxation times of the ^{131}Xe polarization (the square points in Fig. 4) display a similar curing process. We observed qualitatively similar curing processes in all (several tens) of the cells used in this work.

The precise microscopic nature of the curing is not yet understood, but the fact that the glass surface approaches a well-defined limiting state, which appears to be in thermodynamic equilibrium with the Rb metal and vapor in the cell, provides a basis for a quantitative study of wall interactions on these cured surfaces. It is also observed that in some cells the curing improves the signal-to-noise ratio as much as fourfold. This is not fully understood. One possible reason could be that during the curing process the alkali metal destroys surface contaminants like the silicone coatings, which, as will be discussed below, are almost completely depolarizing to the ^{131}Xe nuclear polarization.

B. Temperature dependence of the beat period

We studied the temperature dependence of the beat period by varying the cell temperature, which is monitored by placing a temperature sensor near the cell in the oven. Hot air was blown into the oven, and the flow was

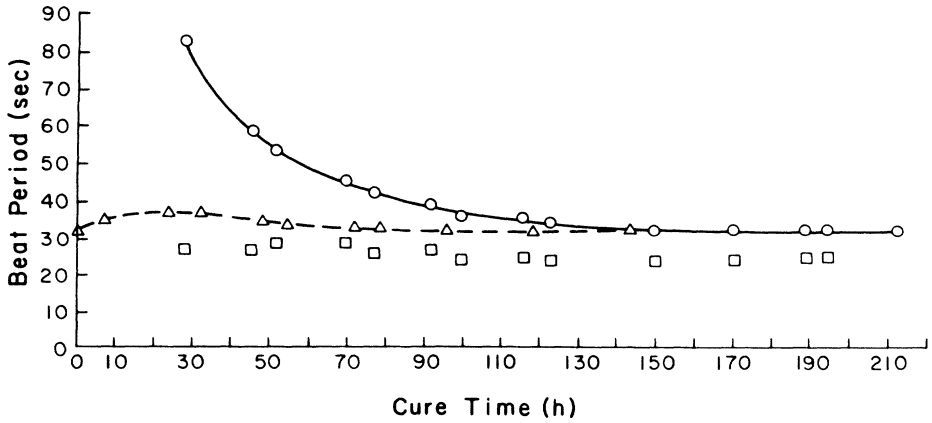

FIG. 4. Evolution of the beat period and relaxation time of a typical Pyrex-glass cell during the curing process.

turbulent enough to ensure a uniform temperature inside the oven. The temperature was stabilized to 0.1 °C by an Omega temperature control system. A small amount of temperature-induced birefringence was induced the glass optics, but this did not contribute to the uncertainty of the measurements. We carefully studied whether the quadrupole splitting depended only on the temperature of the cell or whether it had some hysteresis, that is, whether there was some dependence of the beat frequency or relaxation rate on the past history of the cell. We found that for cured cells with no hydrogen gas the beat frequency and relaxation rates were well-defined functions of temperature.

The beat period $4\pi/|\Delta\Omega_0|$was found to depend only weakly on the cell temperature T. Some representative data (the triangles) are shown in Fig. 5. The observed temperature dependence can be adequately described by assuming that $|\Delta\Omega_0|$ is proportional to an Arrhenius factor $\exp(-E_a/kT)$, with the activation energy given by

$$E_a=-0.03\pm0.01 \text{ eV} . \tag{9}$$

This activation energy is a factor of 10 smaller than the adsorption energy $E=0.3$ eV reported by Ahrens-Botzong, Hess, and Schäfer[14] for bare Pyrex glass. Presumably this means that the surface of cured Pyrex glass is very different from that of bare glass.

C. Dependence of the quadrupole splitting on the cell asymmetry and cell orientation

The beat frequencies depend strongly on the cell geometry, as discussed in connection with Eq. (117) of Ref. 7. For a cylindrical cell, with height h and diameter d, the radian frequency Ω_{mn} of the coherence $|m\rangle\langle n|$, correct to first order in $\langle\theta\rangle$, is

$$\Omega_{mn}=(m-n)\Omega_0+\frac{vA\langle\theta\rangle}{2l}(m^2-n^2)P_2(\cos\psi) , \tag{10}$$

where $P_2(x)=\frac{1}{2}(3x^2-1)$ is the second-order Legendre polynomial, the characteristic cell dimension is

$$\frac{1}{l}=\frac{1}{2h}+\frac{1}{d} , \tag{11}$$

and the cell asymmetry parameter is

$$A=\frac{d-h}{d+2h} . \tag{12}$$

Evaluating (10) for the frequencies of the three $\Delta m=1$ coherences, we find

$$\Omega_{3/2,1/2}=\Omega_0+\Delta\Omega_0P_2(\cos\psi) , \tag{13}$$

$$\Omega_{1/2,-1/2}=\Omega_0 , \tag{14}$$

$$\Omega_{-1/2,-3/2}=\Omega_0-\Delta\Omega_0P_2(\cos\psi) , \tag{15}$$

where

$$\Delta\Omega_0=\frac{vA\langle\theta\rangle}{l} . \tag{16}$$

According to (13)–(16), the sideband splitting frequency should depend as $P_2(\cos\psi)$ on the angle ψ of the cell symmetry axis with respect to the magnetic field direction in the rotating coordinate system. From (8) we see that the tilt angle ψ can easily be changed by varying the rf frequency ω. We have systematically measured the beating frequency as a function of the tilt angle ψ, and the results are shown in Fig. 6. The angular dependence of the data is very close to the predicted dependence on $P_2(\cos\psi)$. The frequencies have been normalized to unity for $\psi=0$. This angular dependence was first noted by Simpson[2] and by Kwon, Mark, and Volk,[4] who physically rotated the cell with respect to the direction of the external magnetic field, rather than tilting the effective nagnetic field with respect to the cell in the rotating coordinate

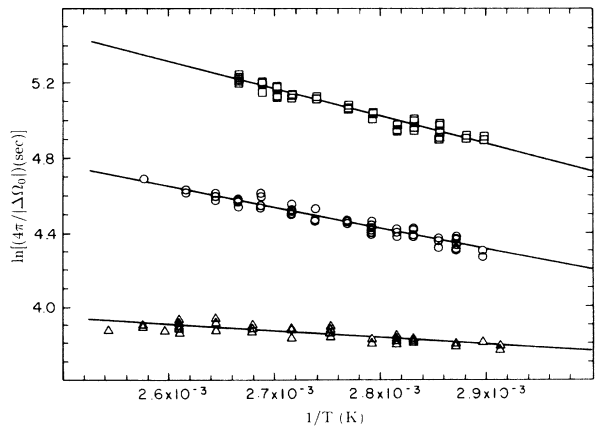

FIG. 5. Temperature dependence of the beat period. The squares and circles represent data corresponding to two different cured states of the same cell that contains H_2 gas (see text). For cells with H_2 gas, the cured state depends on the distribution of alkali-metal droplets and alkali hydride salt within the cell. The triangles represent data taken from a cell that is not intentionally filled with H_2 gas and which has a unique cured state.

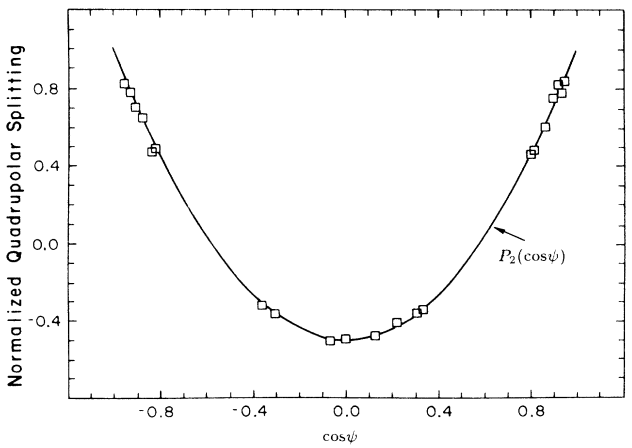

FIG. 6. Dependence of the quadrupole splitting on the orientation of the cell symmetry axis with respect to the quantizing magnetic field.

system, as we have done.

We have also made a series of cylindrical cells with different geometrical shapes, that is, different relative values of the cell diameter d and cell height h. The measured dependence of $\Delta\Omega_0/2\pi$ on the asymmetry parameter $2A/l=1/h-1/d$ is summarized in Fig. 7 for the special case of $\psi=\pi/2$, i.e., $\omega=\omega_0$. All the points are taken from fully cured, hydrogen-free cells. As predicted by (16), the dependence is linear and the slope should be $v|\langle\theta\rangle|$. Using the experimentally determined slope from the data of Fig. 7, and the mean thermal velocity $v=2.32\times10^4$ cm/sec, we find that the mean twist angle per wall interaction of a ^{131}Xe atom is

$$|\langle\theta\rangle|=(38\pm4)\times10^{-6}\text{ rad}\ . \tag{17}$$

The main contribution to the uncertainty of the data is imprecise knowledge about the inner dimension of the cells.

The sideband splittings from the carrier shown in Fig. 3(b) are not quite equal, and this unequal splitting is very reproducible. We believe that the unequal splittings are due to the second-order effects of quadrupole wall interactions. These were discussed in connection with Eqs. (154) and (157) of Ref. 7, which we can use to show that to second-order, (13)–(15) become

$$\Omega_{3/2,1/2}=\Omega_0+\Delta\Omega_0/2\ , \tag{18}$$

$$\Omega_{1/2,-1/2}=\Omega_0+\delta\Omega_0\ , \tag{19}$$

$$\Omega_{-1/2,-3/2}=\Omega_0-\Delta\Omega_0/2\ , \tag{20}$$

where

$$\delta\Omega_0=\frac{3}{16}\frac{(\Delta\Omega_0)^2}{\Omega_0}\ , \tag{21}$$

and we have assumed that $\psi=\pi/2$. Thus, in the second-order approximation, the three Bohr frequencies are no longer equidistant. The slightly unequal spacings obtained from the Fourier spectrum of the transient signals are well described by (18)–(21), as can be seen from Table I. This seems to be the first observation of the effects of second-order interactions on the beat frequencies.

TABLE I. Second-order corrections to the quadrupole splitting $\delta\Omega_0$ are given by (21), which predicts that $16\delta\Omega_0\Omega_0/(3\Delta\Omega_0^2)=1$. Data are taken from three cells, *a*, *b*, and *c*, among which cells *a* and *c* are not filled with H_2 gas, whereas cell *b* is.

Cell	$\frac{\Omega_0}{2\pi}$ (Hz)	$\frac{\Delta\Omega_0}{2\pi}$ (Hz)	$\frac{\delta\Omega_0}{2\pi}$ (Hz)	$\frac{16}{3}\frac{\Omega_0\delta\Omega_0}{(\Delta\Omega_0)^2}$
a	1.250	0.1612	0.0034	0.87
a	0.625	0.1568	0.0072	0.98
a	0.475	0.1568	0.0098	1.01
b	0.155	0.0222	0.0004	0.67
b	0.156	0.0270	0.0010	1.14
c	0.475	0.0630	0.0013	0.83

D. Dependence of quadrupole splitting on the buffer-gas pressure

We studied the dependence of the quadrupole splitting $\Delta\Omega_0/2\pi$ on the buffer-gas pressure. Plotted in Fig. 8 is the quadrupole splitting, normalized to the same cell symmetry, versus N_2 pressure for five cells. As can be seen, there is very little change in the quadrupole splitting as the pressure of N_2 varies between 20 and 240 Torr. At high buffer-gas pressure, due to the short lifetime of the van der Walls molecule RbXe, the transfer of angular momentum between Rb and Xe is very inefficient,[10] and the signal-to-noise ratio is poor. We are therefore unable to measure the relaxation rate at high enough buffer-gas pressures to observe the pressure dependence of the quadrupole splitting predicted in Ref. 7, although the lack of any pressure dependence in the range we were able to study is in agreement with the predictions of Ref. 7.

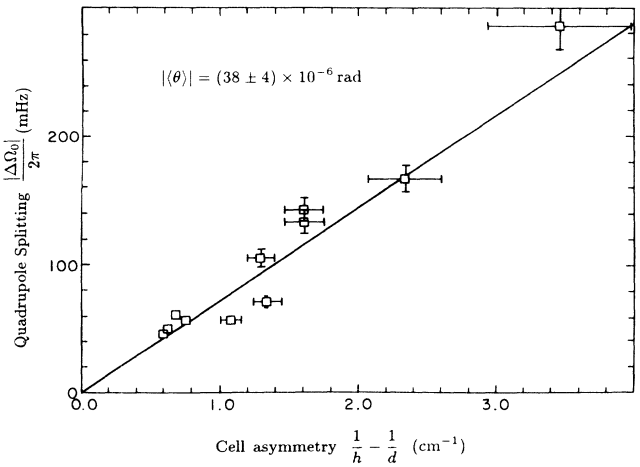

FIG. 7. Measured dependence of the sideband splitting $|\Delta\Omega_0|/2\pi$ on the cell asymmetry parameter $A/2l=h^{-1}-d^{-1}$. According to (16), the slope of this line is $|v\langle\theta\rangle/4\pi|$. All the points are taken at a temperature of 82 °C.

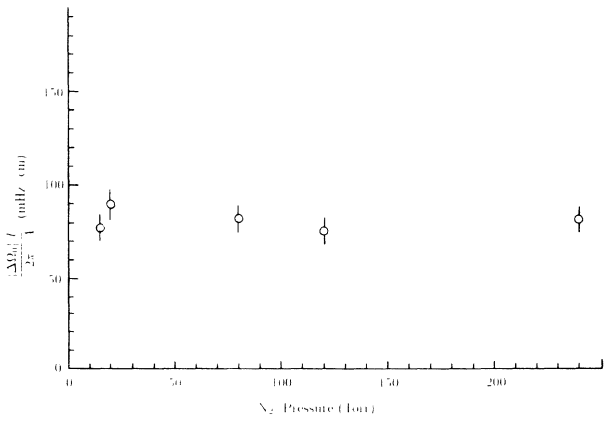

FIG. 8. Dependence of the sideband splitting on the amount of N_2 buffer gas, normalized according to (16) to the same cell geometry. The beating is seen to be independent of the amount of buffer gas in the cell.

E. Wall-induced relaxation rate of spin-polarized ^{131}Xe nuclei

The relaxation of spin-polarized noble-gas nuclei is caused by interactions with alkali-metal atoms in the gas phase, interactions with the cell walls, and by interactions with magnetic field inhomogeneities. For noble-gas atoms that lack nuclear quadrupole moments, the relaxation is mainly due to alkali-metal atoms. At an alkali-metal number density of 10^{12} cm^{-3}, the wall-induced relaxation rate is normally less than 10% of the relaxation rate due to the alkali atoms. However, for ^{131}Xe, which has nuclear quadrupole moment, the wall-induced relaxation normally outweighs the other relaxation mechanisms. For example, the decay of the signal in Fig. 3(a) is almost entirely due to wall interactions since the gas-phase interactions[10] of ^{131}Xe lead to a relaxation time of about 500 sec. According to the theory developed in Ref. 7, the coherences $|3/2\rangle\langle 1/2|$ and $|-1/2\rangle\langle -3/2|$ should relax a factor of 3/2 faster than the coherence $|1/2\rangle\langle -1/2|$, for gas pressures which are not too high, and for cells which are asymmetric enough for the sidebands to be resolved. Our data do not have sufficiently high signal-to-noise ratios to allow us to resolve the relaxation rates of the different coherences, so we will assume that our measured relaxation rates are very nearly equal to the rate for the most slowly decaying coherence $|1/2\rangle\langle -1/2|$. Then according to Eq. (119) of Ref. 7, the pressure-independent contribution to the relaxation rate is

$$\gamma_1=\frac{2}{5}\frac{v\langle\theta^2\rangle}{l}\ , \tag{22}$$

and according to Eq. (146) of Ref. 7, the pressure-dependent part of the relaxation rate at $\psi=\pi/2$ is

$$\gamma_2=\frac{39}{512}\frac{v\langle\theta^2\rangle}{\lambda}\ , \tag{23}$$

where $\langle\theta\rangle$ was defined by (4) and $\langle\theta^2\rangle$ was defined by (5). The mean free path of ^{131}Xe atoms within the gas is λ.

We measured the relaxation time of ^{131}Xe in several cells of the same geometry, with N_2 pressures ranging from 20 to 240 Torr. The difference in relaxation rates was less than a factor of 2. We therefore conclude that the pressure-dependent contribution (23) to the relaxation rate was small compared to the pressure-independent contribution (22). Since in our pressure range, the mean free path $\lambda\sim 10^{-4}$ cm $\ll l$, we have, according to (22) and (23), that $\langle\theta^2\rangle\gg\langle\theta\rangle^2$. That is, the instantaneous magnitude of the fluctuating electric-field gradient is much larger than the ensemble average value.

The relaxation time of transient signals like those of Fig. 3(a) were determined by assuming that the carrier and sideband components of the signals decay with the same exponential time constant. The relaxation time constant for the cell in Fig. 3 is found to be 25 sec. Using this value in (22), we find the mean-squared twist angle

$$\langle\theta^2\rangle=(2.8\pm0.3)\times10^{-6}\ \text{rad}^2\ . \tag{24}$$

Nearly the same value of $\langle\theta^2\rangle$ was obtained for all the cells in Fig. 7. Most of the relaxation is caused by surface interactions, but gas-phase collisions with Rb atoms in the saturated metal vapor make an increasingly important contribution to the relaxation rate as the cell temperature is increased. Because of the difficulty of correcting for the contribution of alkali vapor we have not been able to determine an activation energy for the surface relaxation.

It is possible to be a bit more quantitative about the degree of anisotropy of the field gradients experienced by an atom while it is adsorbed on the wall. We assume that the electric-field gradient acting on the atom has uniaxial symmetry about a unit vector $\mathbf{u}$. Then we can write the twist-rate tensor in the form

$$\dot{\vec{\Theta}}=\tfrac{1}{2}\dot{\theta}_{uu}(3\mathbf{uu}-\mathbf{1})\ , \tag{25}$$

where $\mathbf{1}$ is the unit tensor. We will assume that the magnitude $\dot{\theta}_{uu}$ remains constant, but that the symmetry axis $\mathbf{u}$ varies greatly in direction as the adsorbed atoms move from site to site on the surface, which is microscopically rough because of the atomic structure. Suppose that the symmetry axis $\mathbf{u}$ has a probability

$$W(\beta)d\Omega=\frac{d\Omega}{4\pi}\sum_{l=0}^{\infty}(2l+1)A_lP_l(\cos\beta) \tag{26}$$

to lie in the solid angle increment $d\Omega$ tilted at an angle $\beta=\cos^{-1}(\mathbf{u}\cdot\mathbf{n})$ from the surface-normal direction $\mathbf{n}$. The coefficient of the zeroth-order Legendre polynomial must be $A_0=1$ for normalization. The coefficients A_l of the higher-order Legendre polynomials P_l would also be 1 if $\mathbf{u}$ were always along the surface normal. In fact, experiment shows that $\mathbf{u}$ is nearly isotropic, so that for $l\geq1$, $|A_l|\ll1$. To justify these assertions we replace the time average (4) by an ensemble average over solid angles, and we write

$$\langle\theta\rangle=\tau_s\int d\Omega\ W(\beta)\mathbf{n}\cdot\dot{\vec{\Theta}}\cdot\mathbf{n}=A_2\dot{\theta}_{uu}\tau_s\ . \tag{27}$$

Thus the mean twist angle $\langle\theta\rangle$ is determined only by the coefficient A_2. Similarly, we can write (5) as

$$\begin{aligned}\langle\theta^2\rangle&=\frac{5\tau_c\tau_s^2}{\tau_c+\tau_s}\int d\Omega\ W(\beta)\left[\mathbf{z}\cdot\dot{\vec{\Theta}}\cdot\mathbf{z}\right]^2\\&=\dot{\theta}_{uu}^2\frac{\tau_c\tau_s^2}{\tau_c+\tau_s}(1+\tfrac{10}{7}A_2+\tfrac{18}{7}A_4)\approx\dot{\theta}_{uu}^2\frac{\tau_c\tau_s^2}{\tau_c+\tau_s}\ .\end{aligned} \tag{28}$$

Since we assume that the higher-order asymmetry coefficients A_2 and A_4 are small compared to unity, we have dropped them in writing the last line of (28). Eliminating $\dot{\theta}_{uu}$ from (27) and (28), we find that

$$|A_2|=\left[\frac{\tau_c}{\tau_c+\tau_s}\frac{\langle\theta\rangle^2}{\langle\theta^2\rangle}\right]^{1/2}<\left[\frac{\langle\theta\rangle^2}{\langle\theta^2\rangle}\right]^{1/2}\ . \tag{29}$$

We conclude that

$$|A_2|<0.023\ . \tag{30}$$

Thus the asymmetry coefficient A_2 is small compared to

unity. It is reasonable to assume that the other asymmetry coefficients are small too.

The nature of the buffer gas is known to have a substantial effect on the gas-phase relaxation of ^{129}Xe because of the formation and breakup of van der Waals molecules.[15] In order to rule out the possibility that the relaxation of ^{131}Xe could be due to some bulk effect other than the interactions with Rb atoms, such as the possible formation of van der Waals molecules XeN_2, we measured the relaxation rate of ^{131}Xe in a cell filled with 89.5 Torr of He rather than N_2. We found no appreciable difference between the relaxation of ^{131}Xe in cells with He and N_2 buffer gas.

F. Wall interactions in cells that contain H_2 gas

We have made preliminary studies of cells that were filled with a few Torr of H_2 gas before being sealed off. As was first discovered by Kwon, Mark, and Volk,[4] cells with hydrogen gas added to the nitrogen or helium buffer gas ordinarily used, have substantially slower wall relaxation rates so the beating signals are easier to observe. Presumably this is because the adsorbed Xe atoms have a weaker or shorter-duration quadrupolar coupling with RbH salt, which eventually coats the cell walls, than with the cured Pyrex-glass walls discussed before. The cells that contain H_2 gas also display a curing process. However, in contrast to cells that are free of H_2 gas, the beat period of the "cured" cell will change if the Rb metal and the RbH salt are redistributed on the cell surface using a torch. That is, whereas a unique cured state corresponds to each cell that does not contain H_2 gas, there seem to be many different cured states for a cell that contains H_2 gas. The temperature dependence of the beat period $4\pi/|\Delta\Omega_0|$ for two different cured quasiequilibrium states are shown in Fig. 5 (labeled by squares and circles, respectively). As can be seen, the quadrupole splittings are quite different in the two cured states. Both sets of data seem to be adequately described by assuming that $|\Delta\Omega_0|$ is proportional to an Arrhenius factor $\exp(-E_a/kT)$, with activation energies given by

$$E_a = -0.12 \pm 0.01 \text{ eV} \tag{31}$$

and

$$E_a = -0.09 \pm 0.01 \text{ eV} , \tag{32}$$

respectively. We also found that although the quadrupole splittings for the two cured states in Fig. 5 (squares and circles) differ by almost a factor of 2, the relaxation time for these two states does not vary by more than 25%. This phenomenon is not fully understood. One possible explanation is that when the inner surface of the cell is covered with hydride salt crystals, the local macroscopic surface is determined by the local crystal orientation, which may well be different from the original bare glass surface orientation. This certainly could change $\langle\theta\rangle$. On the other hand, the relaxation time is determined by $\langle\theta^2\rangle$, which is much less sensitive to the local macroscopic surface orientation. Therefore the relaxation time is not expected to change much for different cured states. Using (22), we find the mean-squared twist angle for hydride covered glass surface to be

$$\langle\theta^2\rangle = 1\times10^{-6} \text{ rad}^2 . \tag{33}$$

Due to the lack of a unique cured state for cells that contain H_2 gas, we have been unable to make a quantitative study of the quadrupole splitting for these hydride-coated cells.

G. Effect of wall coatings on spin-polarized ^{131}Xe nuclei

It was found that the relaxation of spin-polarized ^{129}Xe nuclei induced by wall interaction can be substantially reduced by using paraffin or silicone wall coatings. It has been known for some time from the work of the other workers that the same types of coatings slow down the relaxation of spin-polarized alkali-metal atoms and hydrogen atoms.[16,17] However, no studies have been reported on the effects of these wall coatings on the spin-polarized ^{131}Xe nuclei, which have a quadrupole moment. Using the same experimental arrangement and procedures as described in Sec. II, we made a preliminary study of the effects of wall coatings on the spin-polarized ^{131}Xe nuclei. We found that Pyrex-glass walls coated with organic compound such as silicone cause much more rapid spin relaxation for ^{131}Xe nuclei than uncoated glass walls. In studying the difference between coated and uncoated walls, extra care was taken in preparing the cells, and the procedures for making cells will be briefly described here.

The freshly blown Pyrex-glass cells are annealed at $\sim$500 °C for 12 h and then are allowed to cool down in air for a day or so. A mixture of 90% cyclohexane and 10% "surfrasil" (dichlorooctamethyltetrasiloxane) is injected into the cells. After shaking the solution in the cell for about half a minute, the excess is drained off. The cells are then rinsed several times with pure cyclohexane and are allowed to dry overnight. Some variations of the above procedure have been tried. For example, the cells are allowed to sit in the steam of boiling water for about 1 h before the mixture of cyclohexane and Surfrasil is injected. In doing so, the interior surface of the cells is saturated with —OH groups and a thin film of bulk water may also form. According to Holland,[18] this will ensure that the silicone coating agents bond chemically to the hydrated silica substrate. The excess water may lead to polymerization of the silicone coating agent and lead to a thicker coating. Steaming the cells made little difference in the observed relaxation rates, probably because the relative humidity of the air in our laboratory is usually high and adequate to ensure that the surface sites are hydrated before any coating is applied to the surface.[19]

After the cells are coated with Surfrasil, they are connected to a vacuum system. Both liquid nitrogen cold trap and activated Al_2O_3 are used to prevent any possible backstreaming of pump oil vapor from the diffusion pump.[20] The cells are baked at $\sim$200 °C for about 5 h in a vacuum of $\sim5\times10^{-7}$ Torr before some Rb metal is distilled into them. 5 torr of Xe (isotopically enriched to an assay of 70 at. % ^{131}Xe and 10 at. % ^{129}Xe) and 50 Torr of N_2 gas are then added into the cells. The cells are wrapped with wet asbestos when they are pulled off so

that the coating is not damaged by the torch used to seal off the cells.

Representative transient signals obtained by the method described in Sec. II are shown in Fig. 9 for a coated cell A and an uncoated cell B. Each cell contains both ^{129}Xe and ^{131}Xe and the oscillating magnetic field was applied first at the Larmor frequency of ^{131}Xe and approximately 60 sec later at the Larmor frequency of ^{129}Xe. We note that in coated cell the ^{131}Xe signal does not even last long enough to complete the first cycle. This very short relaxation time of ^{131}Xe in coated cells is believed to stem from the high solubility of Xe gas in the wall coating; the Ostwald solubility coefficient is usually great than unity in silicone compounds.[21] The dissolved Xe atom would have a much greater dwell time τ_s on the wall, and if the magnitude of the quadrupolar interaction and the correlation time τ_c are about the same as for an uncoated Pyrex-glass surface, we would expect a much faster damping rate, according to (22) and (5). The diamagnetic coating should have little effect on the relaxation rate of ^{129}Xe, which has no nuclear quadrupole moment, except to hinder the diffusion of ^{129}Xe to paramagnetic sites on the glass wall beneath the silicone coating. Similar results were observed in cells coated with dimethyldichlorosilane.

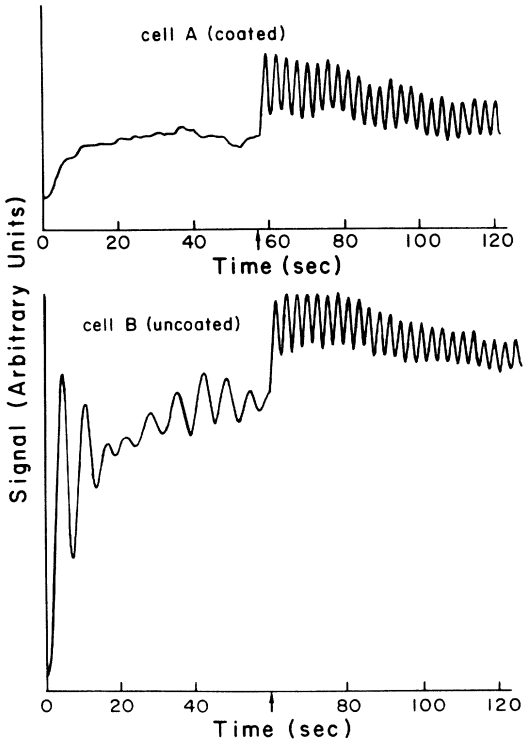

FIG. 9. Both cells A and B are made of Pyrex glass. Cell A is coated with dichlorooctamethyltetrasiloxane and cell B is uncoated. At the instant indicated by the arrow, the oscillating magnetic field switches from the resonance frequency of ^{131}Xe to that of ^{129}Xe. The relaxation rate of ^{129}Xe spin is 9.3×10^{-3} sec^{-1} in cell A and 1.2×10^{-2} sec^{-1} in cell B. Similar results are obtained in cells with dimethyldichlorosilane.

IV. CONCLUSIONS

We have made a first quantitative study of the interactions between the glass surface and adsorbed spin-polarized ^{131}Xe nuclei. The nuclei of ^{131}Xe are polarized by spin exchange collisions with optically pumped Rb atoms in the same Pyrex-glass cell. Some of our most important findings are the following:

(i) Pyrex-glass surfaces reach a unique equilibrium or "cured" state after being exposed to Rb-metal vapor for several days at temperatures of about 80 °C.

(ii) The interaction of the spin-polarized ^{131}Xe atoms with the cured walls is completely dominated by the coupling of the nuclear quadrupole moment to the electric-field gradients experienced by the nuclei while the atoms are adsorbed on the cell wall.

(iii) The electric-field gradients at any surface site are nearly isotropic, and their ensemble averaged mean values are nearly zero. The fluctuating isotropic components of the electric-field gradient cause the nuclear-spin polarization to relax. This relaxation can be attributed to a mean-squared twist angle

$$\langle\theta^2\rangle=(2.8\pm0.3)\times10^{-4}\ \text{rad}^2$$

experienced by the Xe nucleus as a result of a collision with the wall.

(iv) The small residual nonzero mean of the field gradient, which has cylindrical symmetry about the normal to the macroscopic surface of the cell, shifts the $\Delta m=1$ coherence frequencies of the nucleus by different amount and generates beats in the free induction decay of the nuclear polarization. This phenomenon can be characterized microscopically by a mean twist angle

$$|\langle\theta\rangle|=(38\pm4)\times10^{-6}\ \text{rad}$$

experienced by the Xe nucleus about the surface normal direction for each collision with the cell wall. Macroscopically, phenomena due to the coherent wall interaction are proportional to an asymmetry factor (12), which characterizes the anisotropy of the cell. The effects due to the coherent wall interactions are free of any contributions from the isotropic gas-phase interactions, and they provide way to learn about the electric-field gradients experienced by the nuclei of physisorbed noble-gas atoms and about the microscopic roughness of the surface. It would probably be possible to apply these methods to the important xenon-graphite system, which has been extensively studied by other experimental methods and for which detailed theoretical models are available.[22] Beat frequencies like those of Fig. 3 can be used to measure the quadrupole moments of radioactive noble-gas nuclei in experiments analogous to those described by Kitano *et al.*,[23] assuming the electric-field gradients experienced by different isotopes are the same. Wall-induced quadrupole splittings in ^{21}Ne has recently been used by Chupp *et al.*[24] to test local Lorentz invariance.

(v) The magnitude of the mean twist angle depends weakly on temperature and this temperature dependence can be described by an Arrhenius factor $\exp(-E_a/kT)$ with an activation energy

$E_a \sim -0.1\text{eV}$

for hydride-coated Pyrex-glass surface and

$E_a = -0.03\text{eV}$

for cured Pyrex-glass surface, which is not intentionally coated with hydride.

(vi) The quadrupole splitting is independent of buffer-gas N_2 pressure within the range of our measurement (≤ 240 Torr).

(vii) It was found that, in contrast to the case of ^{129}Xe, the relaxation rate of ^{131}Xe nuclear spin is much faster in silicone-coated Pyrex-glass cells than in uncoated ones. This fast relaxation is probably due to the high solubility of Xe gas in silicone compounds, which enhances the quadrupole interaction of ^{131}Xe nuclei with the field gradient at the wall. Our observation of the strong depolarizing effect of silicone coating on spin-polarized ^{131}Xe nuclei will also be useful in the study of polarization of nuclei such as ^{21}Ne, ^{83}Kr, and Rn isotopes which have a quadrupole moment.

ACKNOWLEDGMENTS

This work was supported by the U.S. Air Force Office of Scientific Research under Grant No. 88-0165.

*Present address: Department of Physics, Rutgers University, Newark, NJ 07102.

†Present address: Department of Electronics, Kyoto University, Kyoto, Japan.

‡Present address: Department of Physics, University of Toronto, Toronto, Canada.

[1]D. S. Bayley, I. A. Greenwood, and J. H. Simpson (unpublished).

[2]J. H. Simpson, Bull. Am. Phys. Soc. **23**, 394 (1978).

[3]C. H. Volk, J. G. Mark, and B. Grover, Phys. Rev. A **20**, 2381 (1979).

[4]T. M. Kwon, J. G. Mark, and C. H. Volk, Phys. Rev. A **24**, 1894 (1981).

[5]C. Cohen-Tannoudji, J. Phys. (Paris) **24**, 653 (1963).

[6]F. Masnou-Seeuws and M. Bouchiat, J. Phys. (Paris) **28**, 406 (1967).

[7]Z. Wu, S. Schafer, G. Cates, and W. Happer, Phys. Rev. A **37**, 1161 (1988).

[8]E. J. Campbell, L. W. Buxton, M. R. Keenan, and W. H. Flygare, Phys. Rev. A **24**, 812 (1981).

[9]Z. Wu, W. Happer, and J. Daniels, Phys. Rev. Lett. **59**, 1480 (1987).

[10]X. Zeng, Z. Wu, T. Call, E. Miron, D. Schreiber, and W. Happer, Phys. Rev. A **31**, 260 (1985).

[11]A. L. Bloom, Appl. Opt. **1**, 61 (1962); W. Farr and E. W. Otten, Appl. Phys. **3**, 367 (1974).

[12]Z. Wu, M. Kitano, W. Happer, M. Hou, and J. Daniels, Appl. Opt. **25**, 4483 (1986).

[13]C. P. Slichter, *Principles of Magnetic Resonance* (Springer-Verlag, Berlin, 1978).

[14]R. Ahrens-Botzong, P. Hess, and K. Schäfer, Ber. Bunsenges. Phys. Chem. **77**, 1157 (1973).

[15]J. Hsu, Z. Wu, and W. Happer, Phys. Lett. **112A**, 141 (1985).

[16]H. G. Robinson, E. S. Ensberg, and H. G. Dehmelt, Bull. Am. Phys. Soc. **3**, 9 (1958).

[17]X. Zeng, E. Miron, W. A. van Wijngaarden, D. Schreiber, and W. Happer, Phys. Lett. **96A**, 191 (1983).

[18]L. Holland, *The Properties of Glass Surfaces* (Wiley, New York, 1964).

[19]E. Rochow, *Chemistry of the Silicone* (Wiley, New York, 1946).

[20]M. J. Fulker, M. A. Baker, and L. Laurenson, Vacuum **19**, 556 (1969).

[21]M. Steinberg and B. Manowitz, Ind. Eng. Chem. **51**, 47 (1959).

[22]R. J. Birgenau and P. M. Horn, Science **232**, 329 (1986).

[23]M. Kitano, M. Bourzutschky, F. P. Calaprice, J. Clayhold, W. Happer, and M. Musolf, Phys. Rev. C **34**, 1974 (1986).

[24]T. E. Chupp, R. J. Hoare, R. A. Loveman, E. R. Oteiza, J. M. Richardson, M. E. Wagshul, and A. K. Thompson, Phys. Rev. Lett. **63**, 1541 (1989).